Tertiary Arsine Adducts of Iodoarsines: A Structural and Theoretical Investigation

Simon Petrie,[†] Robert Stranger,*[,†] A. David Rae,[‡] Anthony C. Willis,[‡] Xiangting Zhou,[‡] and S. Bruce Wild*[,‡]

Department of Chemistry, The Faculties, Australian National University, Canberra, Australian Capital Territory 0200, Australia, and Research School of Chemistry, Institute of Advanced Studies, Australian National University, Canberra, Australian Capital Territory 0200, Australia

Received July 6, 2005

The Lewis acid−base adducts $PhMe_2As{\rightarrow}AsPhI_2$, $PhMe_2As{\rightarrow}AsMeI_2$, and $PhMeEtAs{\rightarrow}AsMeI_2$ have been structurally characterized by single-crystal X-ray diffraction, and their structures and bonding investigated by density functional theory calculations at the PBE/TZP level of theory. The adduct $PhMe_2As{\rightarrow}AsPhI_2$ crystallizes in the monoclinic space group $Pna2_1$. The coordination geometry around the arsenic atom of the iodoarsine in the adduct is distorted trigonal bipyramidal with the arsenic atom of the tertiary arsine being almost directly above the arsenic and orthogonal to the T-shaped iodoarsine at a distance of 2.456(1) Å. The nearest intermolecular neighbor to the arsenic of the iodoarsine in the structure is the phenyl group of the tertiary arsine of an adjacent molecule. The adduct $PhMe_2As{\rightarrow}AsMeI_2$ crystallizes in the monoclinic space group $P2_1/c$. The core structure of this adduct is a dimer based on edge-sharing through iodine atoms in the basal $MeAsI_3$ planes of two square pyramids in which the arsenic atoms of the tertiary arsines occupy the apical sites of the pyramids in a trans arrangement within the dimeric unit (As−As 2.4979(5) Å). The adduct $PhMeEtAs{\rightarrow}AsMeI_2$ crystallizes in the space group *Pbca*. Intermolecular contacts between the arsenic of the T-shaped iodoarsine and an iodine of an adjacent molecule trans to the arsenic of the tertiary arsine generate helical $-(-As-I-As-)-_n$ chains of opposite helicity running through the unit cell. The calculations indicate that the molecular orbitals most directly associated with the As−As bonding in the adducts do not show any significant contribution from the virtual orbitals of either arsenic subunit. The theoretical results, which give As−As bond energies of 10−30 kJ mol^{-1} for the three adducts, are consistent with the ready dissociation of the adducts in solution and the importance of intermolecular interactions in stabilizing the complexes in the solid state.

Introduction

Burrows and Turner in 1920 reported the isolation of a number of brightly colored, crystalline adducts of the type $R^1R^2R^3As{\cdot}AsRI_2$, where R^1, R^2, and R^3 were similar or dissimilar alkyl or aryl groups.[1] The compounds completely dissociate in solution, but re-form on evaporation of the solvent. The only other arsine-iodoarsine adducts to be isolated appear to be $Me_3As{\cdot}AsMeI_2$, $Me_3As{\cdot}AsPhI_2$, $n\text{-}Bu_3As{\cdot}AsPhI_2$,[2] $Me_3As{\cdot}AsI_3$, $Me(CH_2AsMe_2)_3{\cdot}AsI_3$,[3] and $1,2\text{-}C_6H_4(AsMe_2)_2{\cdot}AsI_3$.[3,4] Proton NMR data for the latter compounds are consistent with weak bonding between the arsenic atoms in chloroform-d_1, but stronger bonding and a degree of ionization of the arsenic−iodine bonds in the compounds in acetone-d_6.[2,3] Conductivity data for the compounds in nitromethane support the formulation $Me_3As{\rightarrow}AsRI^+I^-$.[2] Because of our interest in the synthesis and applications to asymmetric synthesis of phosphine-stabilized arsenium salts of the type $R_3P{\rightarrow}AsR_2{}^+X^-$, which are most conveniently prepared from reactions of tertiary phosphines with iodoarsines in dichloromethane in the presence of aqueous ammonium hexafluorophosphate,[5] we have carried out a detailed structural and theoretical investigation of the bonding in the Burrows compounds $PhMe_2As{\cdot}AsPhI_2$, $PhMe_2As{\cdot}AsMeI_2$, and $PhMeEtAs{\cdot}AsMeI_2$.

Results and Discussion

Syntheses and Crystal Structures. The complexes $PhMe_2As{\cdot}AsPhI_2$, $PhMe_2As{\cdot}AsMeI_2$, and $PhMeEtAs{\cdot}AsMeI_2$ were prepared by direct combination of the two components in each case, as described by Burrows and Turner;[1] recrystallizations from warm ethanol of the resulting yellow to orange solids furnished crystals suitable for crystal structure determinations. Crystal data, information relating to data collection, and refinement details for the three complexes are given in Table 1. $PhMe_2As{\cdot}AsPhI_2$, mp 36 °C, crystallizes as orange prisms in the monoclinic space group $Pna2_1$ with four molecules in the unit cell. The structure is shown in Figure 1, and important distances and angles are given in Table 2. The three prominent features of the structure are the following: (a) the As−As distance of 2.456(1) Å is similar to the corresponding distance in $Et_3As{\cdot}AsCl_3$, viz., 2.469(3) Å,[6] although in the latter complex the AsCl-*As* atom is five-coordinate, and in certain tetra-alkyl and tetra-aryl diarsines of the type $R_2As-AsR_2$, for example,

* To whom correspondence should be addressed. E-mail: rob.stranger@anu.edu.au (R.S.); sbw@rsc.anu.edu.au (S.B.W.).
[†] Department of Chemistry.
[‡] Research School of Chemistry.

(1) Burrows, G. J.; Turner, E. E. *J. Chem. Soc.* **1920**, *117*, 1373−1383.
(2) Summers, J. C.; Sisler, H. H. *Inorg. Chem.* **1970**, *9*, 862−869.
(3) Hill, J. J.; Levason, W.; Reid, G. *J. Chem. Soc., Dalton Trans.* **2002**, 1188−1192.
(4) Sutton, G. J. *Aust. J. Chem.* **1958**, *11*, 420−425.
(5) Porter, K. A.; Willis, A. C.; Zank, J.; Wild, S. B. *Inorg. Chem.* **2002**, *41*, 6380−6386.
(6) Baum, G.; Greiling, A.; Massa, W.; Hui, B. C.; Lorbeth, J. *Z. Naturforsch., B* **1989**, *44*, 560−564.

10.1021/om0580396 CCC: $33.50
Publication on Web 12/01/2005

Table 1. Crystallographic Data and Experimental Parameters for X-ray Structural Analyses

	$PhMe_2As{\rightarrow}AsPhI_2$	$PhMe_2As{\rightarrow}AsMeI_2$	$PhMeEtAs{\rightarrow}AsMeI_2$
empirical formula	$C_{14}H_{16}As_2I_2$	$C_9H_{14}As_2I_2$	$C_{10}H_{16}As_2I_2$
fw, g mol^{-1}	587.93	525.86	539.89
cryst syst	orthorhombic	monoclinic	orthorhombic
space group	*Pna*2$_1$	*P*2$_1$/*c*	*Pbca*
a, Å	16.4722(3)	9.5721(1)	7.7215(1)
b Å	9.9146(2)	7.1931(1)	15.6703(2)
c Å	10.4624(2)	20.9867(3)	25.6240(4)
β, deg		97.5745(4)	
V, Å^3	1708.67(6)	1432.39(3)	3100.46(7)
Z	4	4	8
D_{calcd}, g cm^{-3}	2.285	2.438	2.313
cryst size, mm	0.40 × 0.34 × 0.22	0.44 × 0.24 × 0.17	0.42 × 0.25 × 0.07
μ, mm^{-1}	7.508	8.940	8.263
instrument	Nonius Kappa CCD	Nonius Kappa CCD	Nonius Kappa CCD
radiation	Mo Kα	Mo Kα	Mo Kα
no. of unique reflns	3826	3286	3530
no. of reflns obsd ($I > 3\sigma(I)$)	3342	2765	2105
temp, K	200	200	200
struct refinement	RAELS2000[13b]	CRYSTALS[13a]	CRYSTALS[13a]
final R_1, wR_2	0.023, 0.022	0.0286, 0.0326	0.0179, 0.0186

$Me_2As{-}AsMe_2$, 2.429(1) Å,[7] and $Mes_2As{-}AsMes_2$, 2.472(3) Å (Mes = mesityl);[8] (b) the coordination geometry around As(2) of the iodoarsine is distorted trigonal pyramidal with the arsenic atom of the tertiary arsine group, As(1), being almost directly above As(2) in the trigonal plane of the T-shaped iodoarsine; and (c) the nearest intermolecular neighboring atoms to As(2) are C(4), C(5), and C(6) of the phenyl group of the tertiary arsine group of an adjacent adduct (Figure 1). This weak As$-\eta^3$-arene interaction (mean As$-$C: ca. 3.7 Å) is analogous to those observed in the crystal structures of $SbPhX_2$ (X = Cl, Br, I); the corresponding intermolecular Sb$-$C distance in $SbPhI_2$ is ca. 3.5 Å.[9] In the complexes $C_6Me_6{\cdot}2AsCl_3$ and $C_6Et_6{\cdot}2AsCl_3$, the arsenic atoms are η^6-coordinated to the arene rings from both sides at distances of 3.20 and 3.14 Å, respectively.[10]

The adduct $PhMe_2As{\cdot}AsMeI_2$, yellow plates, mp 93 °C, crystallizes in the monoclinic space group *P*2$_1$/*c* with four molecules in the unit cell. The core structure of the adduct is a dimer based on edge-sharing through iodine atoms in the basal $MeAsI_3$ planes of two square pyramids; the arsenic atoms of the tertiary arsine groups occupy the apical sites of the pyramids and are trans to each other in the dimeric unit (Figure 2). Important distances and angles in the structure are listed in Table 2. The terminal iodine atoms are trans to each other (as are the methyl groups) in the dimer with As(2)$-$I(2), As(2)$^1-$I(2)^1 being 2.9829(2) Å; the bridging arsenic$-$iodine distances are shorter, viz., As(2)$-$I(1), As(2)$^1-$I(1)^1 2.7416(4) Å. The As(1)$-$As(2) distances in the dimer are 2.4979(5) Å, and the angles subtended at As(2) are close to the 90° and 180° expected for a square pyramid. The $X_2As(\mu\text{-}X)AsX_2$ core structure with trans axial substituents has also been found in the structures of $[Me_3P{\cdot}AsCl_3]_2$,[3] $[Et_3P{\cdot}AsCl_3]_2$,[6] and $[Me_3P{\cdot}SbI_3]_2{\cdot}THF$.[11] There appear to be no significant intermolecular interactions in $[Et_3P{\cdot}AsCl_3]_2$, but in $[Me_3P{\cdot}AsCl_3]_2$ there is an As$\cdots$Cl interaction at ca. 3.43 Å [sum of van der Waals' radii for As and Cl: 3.60 Å] trans to phosphorus that weakly associates the dimeric units into a polymeric staircase arrangement. In $[Me_3P{\cdot}SbI_3]_2{\cdot}THF$, two terminal iodine atoms of each dimer form weak bridges to the antimony atoms of adjacent dimers to give a weakly bound polymer in which the coordination geometry around each antimony is octahedral to within 10° of the idealized values. In $[PhMe_2As{\cdot}AsMeI_2]_2$, the coordination geometry around As(2)

Table 2. Selected Bond Distances (Å) and Angles (deg) in the Adducts

	$PhMe_2As{\rightarrow}AsPhI_2$	$PhMe_2As{\rightarrow}AsMeI_2$	$PhMeEtAs{\rightarrow}AsMeI_2$
As1$-$As2	2.456(1)	2.4979(5)	2.4733(5)
As2$-$I1	2.877(1)	2.7416(4)	2.7960(6)
As2$-$I2	2.842(1)	2.9829(4)	2.9261(4)
As2$-$C9	1.964(4)	1.988(3)	1.978(4)
As1$-$As2$-$I1	85.2(1)	93.74(1)	86.99(2)
As1$-$As2$-$I2	92.0(1)	84.19(1)	91.15(2)
As1$-$As2$-$C9	101.0(1)	93.2(1)	96.1(1)
I1$-$As2$-$I2	174.4(1)	175.68(1)	177.00(2)
I1$-$As2$-$C9	92.7(1)	93.9(1)	92.2(1)
I2$-$As2$-$C9	92.5(1)	90.0(1)	90.3(1)

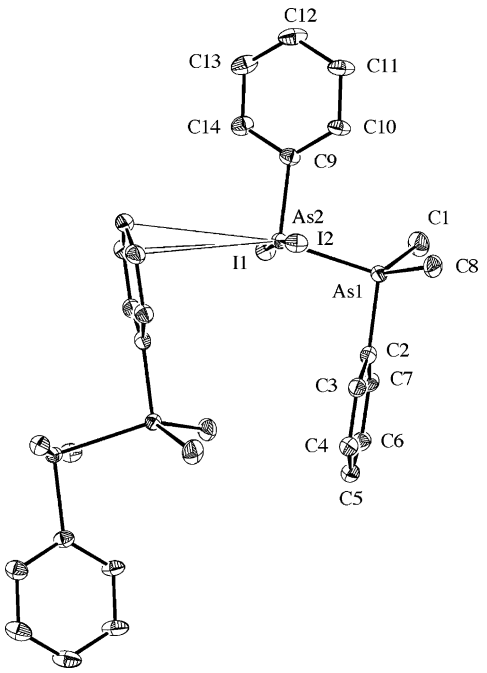

Figure 1. Anisotropic displacement ellipsoid plot of $PhMe_2As{\rightarrow}AsPhI_2$ showing 30% probability ellipsoids for non-hydrogen atoms.

(7) Mundt, O.; Riffel, H.; Becker, G.; Simon, A. *Z. Naturforsch., B* **1988**, *43*, 952−958.
(8) Chen, H.; Olmstead, M. M.; Pestana, D. C.; Power, P. P. *Inorg. Chem.* **1991**, *30*, 1783−1787.
(9) Mundt, O.; Becker, G.; Stadelmann, H.; Thurn, H. *Z. Anorg. Allg. Chem.* **1992**, *617*, 59−71.
(10) Schmidbaur, H.; Novak, R.; Steigelmann, O.; Müller, G. *Chem. Ber.* **1990**, *123*, 1221−1226.
(11) Clegg, W.; Elsegood, M. R. J.; Graham, V.; Norman, N. C.; Pickett, N. L.; Tavakkoli, K. *J. Chem. Soc., Dalton Trans.* **1994**, 1743−1751.

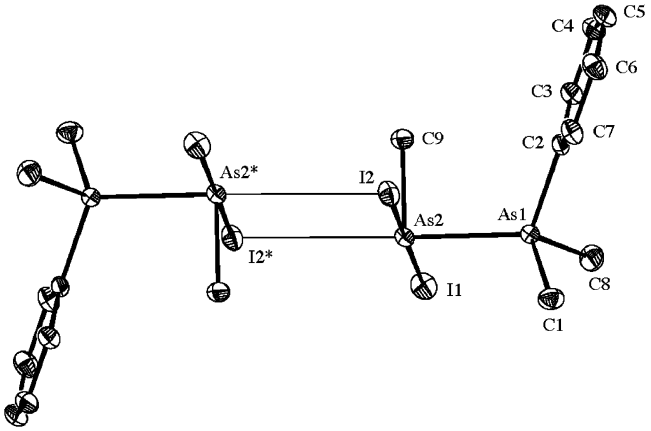

Figure 2. Displacement ellipsoid diagram of $[PhMe_2As{\rightarrow}AsMeI_2]_2$ showing 30% probability levels for non-hydrogen atoms.

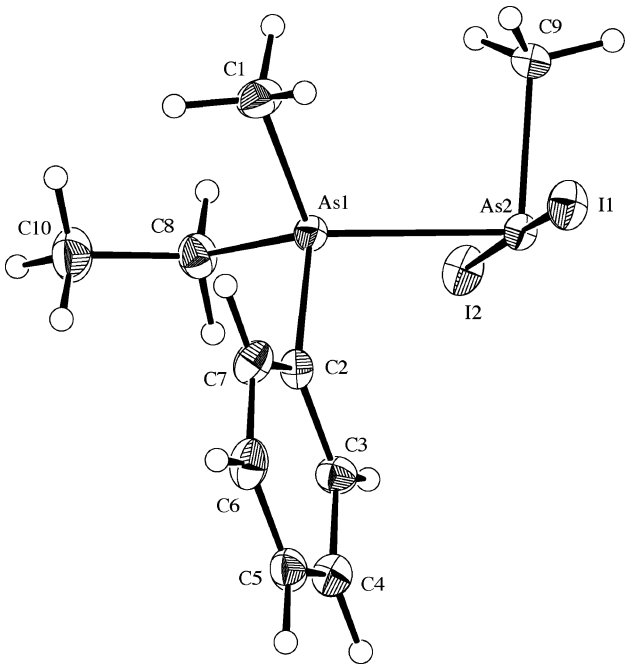

Figure 3. Displacement ellipsoid diagram for $PhMeEtAs{\rightarrow}AsMeI_2$ showing 30% probability levels for non-hydrogen atoms.

is similar, the intermolecular As···I distances being 3.4380(4) Å in the polymeric structure (Figure 2).

The adduct $PhMeEtAs{\cdot}AsMeI_2$, yellow needles, mp 84 °C, crystallizes in the achiral space group *Pbca*; the crystallographic asymmetric unit consists of one molecule of the adduct in which the distances and angles correspond closely with those in $PhMe_2As{\cdot}AsMeI_2$ (Table 2). The structure is shown in Figure 3. Intermolecular contacts between As(2) and the I(2) atoms of adjacent molecules give rise to helical $-(-As-I-As-)-_n$ chains running through the unit cell (Figure 4). The chains are created by a 2_1 axis $^1/_2 + x$, $^1/_2 - y$, $-z$. The crystallographic inversion center creates strands of opposite helicity in the lattice.

Density Functional Theory (DFT) Calculations. Isolation of Vacuum-Phase Monomeric Stationary Points. Geometry optimizations at the PBE/TZP level of theory[14] have delivered geometries for the "monomers" $PhMe_2As{\rightarrow}AsPhI_2$, $PhMe_2As{\rightarrow}AsMeI_2$, and $PhEtMeAs{\rightarrow}AsMeI_2$ that show close similarities with those apparent within the crystals. Critical features of

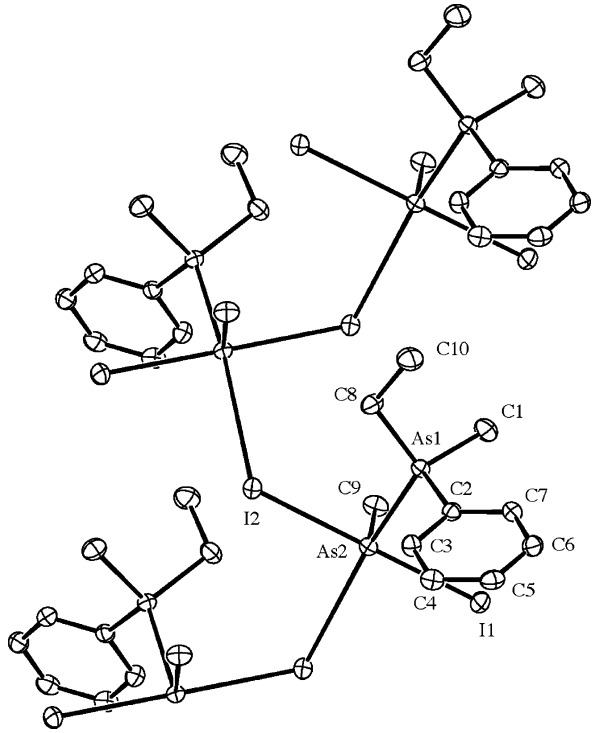

Figure 4. Packing in $[PhMeEtAs{\rightarrow}AsMeI_2]_n$ that gives rise to alternating helical chains of molecules in the lattice. Ellipsoids show 30% probability levels.

the optimized "crystal-conformation monomer" geometries are summarized in Figure 5. The correspondence between the crystallographic and calculated geometries is good: As−As and As−C lengths are within ±2.6% of the crystallographically determined values, but the As−I lengths are more erratic. The disparity in the As−I distances most likely reflects the central role that these interactions play in "knitting" adjacent molecules together within the larger crystalline structure and the absence of intermolecular contacts being included in the calculations.

In an attempt to understand the bonding within the $R^1R^2R^3$-$As{\rightarrow}AsRI_2$ adducts, a fragment-based analysis of the As−As interaction was undertaken where the $R^1R^2R^3As$ and $AsRI_2$ components were treated separately. This approach[15−19] uses individual single-point calculations with the geometry of each subunit being frozen at the geometry optimized within the $R^1R^2R^3As{\rightarrow}AsRI_2$ molecule; the molecular orbitals thus obtained for each subunit are then employed in place of the regular atomic orbitals in a subsequent single-point calculation on $R^1R^2R^3As{\rightarrow}AsRI_2$.[15−19] The data from these calculations are detailed in Table 4. The results suggest that the attractive interaction between the subunits within $R^1R^2R^3As{\rightarrow}AsRI_2$ is the sum of an approximately equal measure of electrostatic (ΔV_{elstat}) and orbital (ΔE_{orbit}) contributions. (Note that the "electrostatic" contribution cannot be straightforwardly regarded

(12) SIR92: Altomare, A.; Cascarano, G.; Giacovazzo, C.; Guagliardi, A.; Burla, M. C.; Polidori, G.; Camalli, M. *J. Appl. Crystallogr.* **1994**, *27*, 435.

(13) (a) Watkin, D. J.; Prout, C. K.; Carruthers, J. R.; Betteridge, P. W.; Cooper, R. I. *CRYSTALS*, Issue 11; Chemical Crystallography Laboratory: Oxford, U.K., 2001. (b) Rae, A. D. *RAELS2000*, A Comprehensive Constrained Least-Squares Refinement Program; Australian National University: Canberra, ACT 0200, Australia, 2000.

(14) Perdew, J. P.; Burke, K.; Ernzerhof. *Phys. Rev. Lett.* **1997**, *78*, 1396.

(15) Morokuma, K. J. *Chem. Phys.* **1971**, *55*, 1236−1244.

(16) Kitaura, K.; Morokuma, K. Int. *J. Quantum Chem.* **1976**, *10*, 325−340.

(17) Ziegler, T.; Rauk, A. *Inorg. Chem.* **1979**, *18*, 1558−1565.

(18) Ziegler, T.; Rauk, A. *Inorg. Chem.* **1979**, *18*, 1755−1759.

(19) Bickelhaupt, F. M.; Baerends, E. J. In *Reviews in Computational Chemistry*; Lipkowitz, K. B., Boyd, D. B., Eds.; Wiley-VCH: New York, 2000; Vol. 15, p 1.

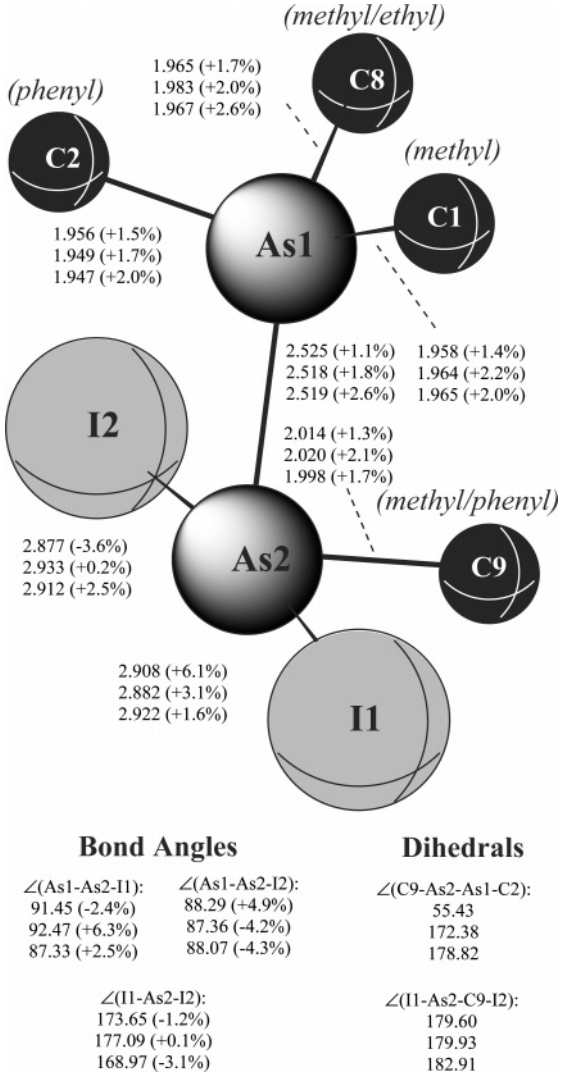

Figure 5. Principal distances (Å) and angles (deg) for PBE/TZP-optimized geometries of $PhMe_2As{\rightarrow}AsPhI_2$, $PhMe_2As{\rightarrow}AsMeI_2$, and $PhMeEtAs{\rightarrow}AsMeI_2$. Atom labeling is consistent with that used for crystal structures; values in parentheses indicate deviations for crystal structure data.

as "ionic", nor the "orbital" contribution as "covalent": a coordinate covalent interaction would be indicated predominantly through the orbital contribution, since the ionic character in such an interaction arises from the overlap of an occupied orbital on one fragment with a vacant orbital on the other fragment.) The BDE obtained from the fragment-based analysis in each case is lower, viz., 170−185 kJ mol^{-1}, than either of the electrostatic or orbital contributions to the overall bond energy due to the rather large Pauli repulsion term for each adduct. The qualitative assignment of the $R^1R^2R^3As{\rightarrow}AsRI_2$ interaction as a coordinate bond is supported by the Mulliken and Voronoi charge descriptions of the adduct compared to the charge descriptions of the isolated fragments. The occupied molecular orbitals most directly associated with either As atom, however, show no significant contribution (<5%) from the virtual orbitals of the other As-containing subunit, which indicates that within the gas-phase monomer any tendency toward coordinate covalent bonding between the subunits is weak. This aspect of the As−As bonding is addressed below.

The bond strengths obtained through the fragment-based calculations embodied in Table 3 are sizable. However, these are *vertical* bond strengths (i.e., ignoring any geometric relaxation of the separated fragments). A different picture is obtained when *adiabatic* bond strengths are assessed through optimization of the separated fragments $R^1R^2R^3As$ and $AsRI_2$. In absolute thermodynamic terms, none of the three adducts has an As−As bond strength (for the monomeric complex) exceeding 30 kJ mol^{-1} at the chosen level of theory. The bond strengths obtained are also insensitive to inclusion or exclusion of ZORA scalar relativistic corrections.[20,21]

Table 3. Bond Energy Decomposition Values for the As−As Bonds in $PhMe_2As{\rightarrow}AsPhI_2$ (A), $PhMe_2As{\rightarrow}AsMeI_2$ (B), and $PhEtMeAs{\rightarrow}AsMeI_2$ (C)[a]

	energy (kJ mol^{-1})		
bond energy term	A	B	C
total Pauli repulsion, ΔE_{Pauli}[b]	691	634	662
electrostatic interaction, ΔV_{elstat}[b]	−426	−401	−416
total steric interaction, ΔE_0[b]	265	233	246
total orbital interactions, ΔE_{orbit}[b]	−443	−404	−428
bond dissociation energy $(BDE)_{vertical}$[c]	178	172	182
$BDE_{adiabatic}$[d]	13	21	29
$BDE_{ad(rel)}$[d,e]	9	17	26

[a] B-LYP/TZP fragment-based calculations on the crystal structure conformations of the adducts. [b] Terms used are those defined in the analysis scheme of Bickelhaupt and Baerends.[16] In accordance with thermochemical conventions, a negative energy value indicates an attractive contribution to the interaction. [c] BDE vertical: dissociation energy, without rearrangement into separated fragments. [d] BDE adiabatic: dissociation energy calculated from the total energies of geometry-optimized separated fragments. [e] $BDE_{ad(rel)}$: dissociation energy including a scalar relativistic correction obtained according to the ZORA formalism.[20]

The large difference seen between vertical and adiabatic bond strengths for each complex arises from the substantial geometric distortion of the $AsRI_2$ subunit upon complexation. The optimized geometry of the isolated $AsRI_2$ group is essentially pyramidal (for $AsCH_3I_2$, ∠(I−As−I) = 104.6° and ∠(I−As−C−I) = 105.7°), in contrast to the near-coplanarity of the As−I and As−C bonds and the almost linear I−As−I arrangement within the adducts (Figure 5). This "flattening" of the $AsRI_2$ group is highly energy demanding (ca. 130 kJ mol^{-1} for $AsMeI_2$ and ca. 140 kJ mol^{-1} for $AsPhI_2$), whereas distortion of the $R^1R^2R^3As$ group within the complex consumes ca. 25 kJ mol^{-1}. Thus, the strain energy within the $AsRI_2$ group upon complexation is the principal source of the large difference between vertical and adiabatic BDE values.

The structures obtained for the $R^1R^2R^3As{\rightarrow}AsRI_2$ adducts are highly reminiscent of that of the $Me_3Sb{\rightarrow}SbMeI_2$ adduct characterized by Breunig and co-workers[22] and of the many other compounds of the generic formula $R_3M{\rightarrow}M'R'_nX_{3-n}$ (M, M′ = P, As, Sb; X = Cl, I).[2,11,22,23] Although the present calculations on the monomeric $R^1R^2R^3As{\rightarrow}AsRI_2$ adducts reproduce most of the features of the crystal structures, they do not account for the substantial short−long As−I bond length alternation that is seen with particular clarity in $PhMe_2As{\rightarrow}AsMeI_2$, viz., As2−I1 = 2.742 Å, As2−I2 = 2.983 Å, and in $Me_3Sb{\rightarrow}SbMeI_2$, viz., Sb−I = 2.913 and 3.093 Å.[22,23] This alternation in bond lengths is clearly associated with the intermolecular interactions in the solid state.

Conformers of $PhMe_2As{\rightarrow}AsMeI_2$ and $PhEtMeAs{\rightarrow}AsMeI_2$. The calculations described above explore the bonding

(20) van Lenthe, E.; Baerends, E. J.; Snijders, J. G. *J. Chem. Phys.* **1993**, *99*, 4597−4610.
(21) van Lenthe, E.; Ehlers, A. E.; Baerends, E.-J. *J. Chem. Phys.* **1999**, *110*, 8943−8953.
(22) Breunig, H. J.; Ebert, K. H.; Gülec, S.; Dräger, M.; Sowerby, D. B.; Begley, M. J.; Behrens, U. *J. Organomet. Chem.* **1992**, *427*, 39−48.
(23) Breunig, H. J.; Denker, M.; Ebert, K. H. *J. Chem. Soc., Chem. Commun.* **1994**, 875−876.

Table 4. Angles (deg) and Energies (kJ mol^{-1}) for the Conformers of $PhMe_2As{\rightarrow}AsMeI_2$ and $PhEtMeAs{\rightarrow}AsMeI_2$

C2−As1−As2−C9	I1−As2−I2	I1−As2−C9−As1[a]	E_{rel}[b]	BDE[c]	$E_{rel(ZORA)}$[b]	BDE_{ZORA}[c]
		$PhMe_2As{\rightarrow}AsMeI_2$				
55.4	173.7	88.6	0.0	21.0	0.0	16.5
177.0	176.3	88.8	−4.6	25.6	−5.0	21.5
33.4	102.4	84.9	−1.3	22.3	−5.8	22.3
36.4	102.3	−88.3	0.3	20.7	−5.1	21.7
157.2	102.9	91.1	3.2	17.8	−2.0	18.5
154.6	102.5	−89.9	3.1	17.9	−2.3	18.8
−88.1	102.5	86.0	0.4	20.6	−4.3	20.8
−87.7	102.4	−92.7	6.0	15.0	0.7	15.9
		$PhEtMeAs{\rightarrow}AsMeI_2$				
172.4	177.1	87.5	0.0	29.1	0.0	25.7
−64.4	173.9	88.9	4.9	24.1	4.8	20.9
71.9	174.4	94.4	5.3	23.8	6.3	19.3
168.7	102.9	87.7	9.1	20.0	5.7	19.9
165.1	102.7	−88.0	9.7	19.4	5.9	19.8
−28.3	102.3	87.3	7.6	21.5	3.8	21.8
−31.1	102.9	−86.5	5.7	23.4	2.4	23.3
58.7	102.1	88.6	7.2	21.9	3.2	22.5
76.1	102.8	−86.1	5.6	23.4	2.5	23.2

[a] For the planar-$AsMeI_2$ adducts I1−As2−I2 is ca. 174° (I1 is the iodine atom with the shorter As−I distance); for pyramidal-$AsMeI_2$ adducts I1−As2−I2 is ca. 102° (I1 is the equatorial and I2 the axial iodine atom). [b] Total energy of species, as expressed relative to that of the monomer most closely resembling the observed structure. [c] Dissociation energy for the As−As bond (see text).

within the $R^1R^2R^3As{\rightarrow}AsRI_2$ monomers, which show a close correspondence with the structures of subunits within the crystal structures. The conformations of the monomers within the crystal lattices, however, may not represent the most stable conformations in the gas phase. The $R^1R^2R^3As{\rightarrow}AsRI_2$ structural motif exhibits a rich conformational isomerism, as summarized in Table 4. We have isolated two sets of rotational conformers for $PhMe_2As{\rightarrow}AsMeI_2$ and $PhEtMeAs{\rightarrow}AsMeI_2$, as represented by the structures in Figure 6. In the planar-$AsMeI_2$ set, which includes the subunits seen in most crystal structures, the T-shaped $AsMeI_2$ group has both I atoms in equatorial positions with respect to the As−As axis. Interconversions between conformers within this group are effected by rotations about the As−As axis; the C9−As2−As1−C2 dihedral angle (which describes the torsional relationship between the carbon atom of the $AsMeI_2$ group and the methyl group ipso-aromatic carbon atom of the $PhMe_2As$ or PhMeEtAs groups) provides a useful descriptor for the conformers having the planar-$AsMe_2$ group. The second set of conformers contain a pyramidal-$AsMeI_2$ group, in which one I atom of the group is effectively equatorial, and the other axial, relative to the As−As axis. Within this set of pyramidal-$AsMeI_2$ conformers, the degree of rotation about the As−As axis can be described by the dihedral angle C2−As1−As2−C9; the possibility of either iodine atom occupying the axial position is described by the dihedral angle I1−As2−C9−As1.

According to the relative energies listed in Table 4, the structure of $PhMe_2As{\rightarrow}AsMeI_2$ found within the crystal lattice is not the most stable conformer. Ignoring relativistic corrections, the preferred structure for this molecule has a planar-$AsMeI_2$ group in which there is an anti relationship between C2 and C9. When ZORA[20] relativistic corrections are included, however, the pyramidal-$AsMeI_2$ structures are systematically favored, with one of the gauche C2/C9 conformers having the lowest energy. Regardless of whether relativistic corrections are included or not, the potential energy surface for the molecule is almost flat (although we have not verified this lack of contrast by isolating the isomerization transition states), since all of the eight structures located for the adduct are ensconsed within a potential energy span of <11 kJ mol^{-1}. These results are in only moderate agreement with experiment: the ZORA-corrected calculations correctly predict the C2/C9 torsional relationship to be optimized at C9−As2−As1−C2 ca. 30°, but the lowest energy, pyramidal-$AsMeI_2$ structure that exhibits this conformation has an As−As length of 3.160 Å, which is ca. 0.65 Å longer than the crystallographic value. In contrast, the calculations neglecting ZORA corrections fare better for the As−As bond length (0.06 Å too long) but show a preference for the wrong (anti) C2/C9 torsional relationship. Each structural type enjoys only partial success in predicting the As−I bond lengths: both As−I bonds in the lowest energy planar-$AsMeI_2$ structure are only marginally shorter than the "long" As−I seen in the crystal structure, while the As−I bonds in the pyramidal-$AsMeI_2$ structure are close to the crystallographic, "short" As−I distance. Neither of the two structures calculated correctly reproduces the As−I bond length alternation seen in the crystal structure.

For $PhEtMeAs{\rightarrow}AsMeI_2$, the situation is more straightforward: the crystal structure conformation corresponds to the lowest energy calculated structure in both the ZORA-corrected and uncorrected calculations. Again, the span in total energies is modest, 10 kJ mol^{-1} or less, and, again, the inclusion of ZORA corrections favors pyramidal-$MeAsI_2$ structures by a small margin.

Why are there large differences between the lowest energy ZORA-corrected geometries for $PhMe_2As{\rightarrow}AsMeI_2$ and $PhEtMeAs{\rightarrow}AsMeI_2$, as well as between the ZORA-corrected and uncorrected geometries for $PhEtMeAs{\rightarrow}AsMeI_2$ itself? We surmise that these disparities originate in the reluctance of the $AsMeI_2$ group in the adducts to undergo distortion from pyramidal to planar geometry. The strain energy associated with this distortion consumes almost all of the energy released by the As−As bond formation, as is evident from a comparison of the vertical and adiabatic BDEs for the adducts (Table 3). Consequently, the As−As interactions within the planar-$AsMeI_2$ adducts are only as strong, overall, as the van der Waals-type interactions between the As atoms in the pyramidal-$AsMeI_2$ adducts, with the result that the potential energy surface for the overall system is unusually flat.

Calculations on the Dimer $(PhMe_2As{\rightarrow}AsMeI_2)_2$. To explore the drive toward crystallization, we have performed calculations on the dimeric species $(PhMe_2As{\rightarrow}AsMeI_2)_2$, as well as on the smaller subunits $PhMe_2As{\rightarrow}As(Me)(I)$-$\mu(I)_2$-AsMeI and IMeAs-$\mu(I)_2$-AsMeI. Geometries for the three species are identified in Figure 7. A satisfying transition from pyramidal- toward planar-$AsMeI_2$ groups occurs as $PhMe_2As$ groups (A) are added to the IMeAs-$\mu(I)_2$-AsMeI core (BB). For

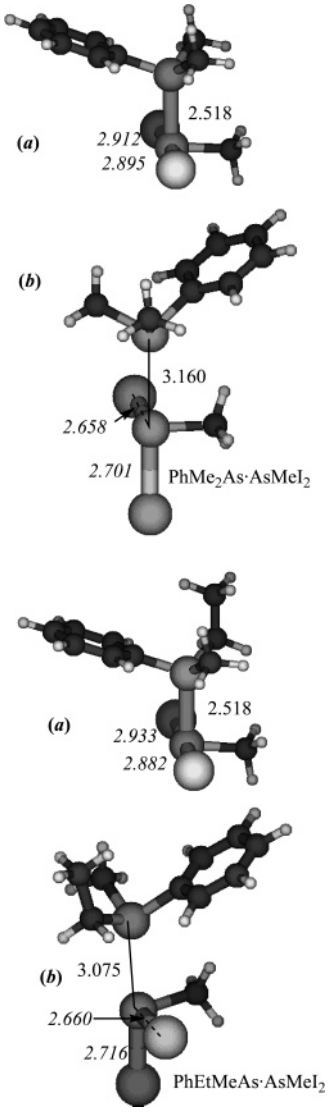

Figure 6. Lowest energy, PBE/TZP-optimized structures of planar-$AsMeI_2$ (a) and pyramidal-$AsMeI_2$ (b) conformers of $PhMe_2As{\rightarrow}AsMeI_2$ and $PhMeEtAs{\rightarrow}AsMeI_2$. The planar-$AsMeI_2$ structures represent the global minima when relativistic corrections are excluded; the pyramidal-$AsMeI_2$ structure for $PhMe_2As{\rightarrow}AsMeI_2$ is preferred when ZORA relativistic corrections are included in the calculations.

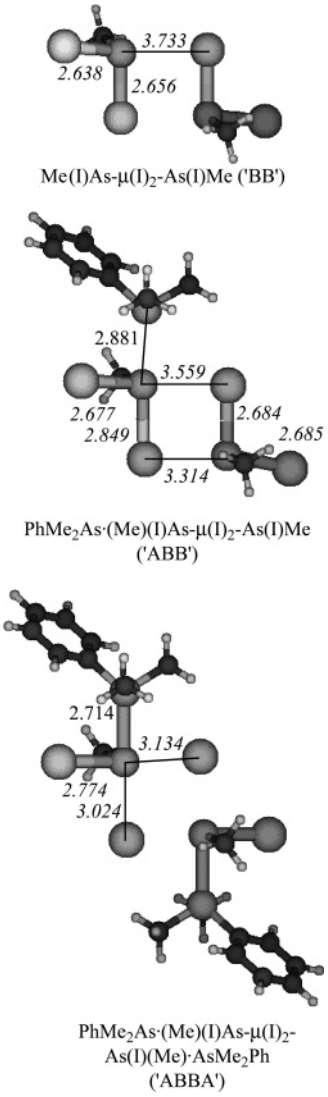

Figure 7. Lowest energy, PBE/TZP-optimized structures for $(PhMe_2As{\rightarrow}AsMeI_2)_2$ (ABBA) and subunits ABB and BB. For BB and ABBA, C_i symmetry was imposed on the structure.

BB, the composition as a loosely interacting pair of pyramidal molecules is clear: the intermolecular As−I distances of 3.73 Å are >1 Å longer than the corresponding intramolecular bond lengths. Considerable contraction of this "intermolecular gap" occurs when one and then two A molecules are added to BB, and this is accompanied by a substantial stretching of the axial As−I bonds upon $PhMe_2As$ complexation and a lesser but progressive lengthening of the equatorial As−I bonds (ultimately, from 2.64 to 2.74 Å). The As_2I_4 skeleton within the largest optimized structure, ABBA, does not show exact correspondence with the crystal structure geometry; the calculated geometry appears to equivocate between planar- and pyramidal-$AsMeI_2$ components, whereas in the crystal structure the $AsMeI_2$ groups are unambiguously planar. The linear alternation of short and long As−I bonds is reproduced well in the calculated ABBA structure, with the short bond length being in particularly good agreement with the crystal structure value of 2.742 Å. The As−As bond lengths in the ABBA calculation are poorer (when assessed against the crystallographic values) than the calculated As−As bond length in the AB monomer in the crystal structure conformation, but this apparent failing is better viewed in the context of the performance of structure ABB, which contains a yet longer As−As distance. The addition of a further $PhMe_2As$ group to ABB gives a substantial improvement in all of the As−As and As−I distances, and it is reasonable to surmise that the residual shortcomings in the calculated ABBA geometry are due to the neglect of longer range interactions, such as the continuation of the −I−As(I)−I− bonding pattern seen in the crystal structures.

The energetic aspects concerning the dimerization of $PhMe_2As{\rightarrow}AsMeI_2$ are given in Table 5. Although none of the individual As−As (or As−I) bonds within the larger species ABB and ABBA exhibit (vertical) bond energy contributions as large as those observed for the As−As bonding in AB, the adiabatic As−As BDE values for the larger species consistently exceed that of the monomer, *despite the larger As−As separations in ABB and ABBA compared to AB*. This latter observation reinforces our contention that the intermolecular interactions within the crystal are crucial to the structural integrity of $PhMe_2As{\rightarrow}AsMeI_2$ and related compounds, and is consistent with the original observation[1] that the molecular weights of certain of these adducts in solution are ca. one-half of their formula

Table 5. Calculated Bond Energy Contributions (kJ mol^{-1}) for Adducts and Components $PhMe_2As$ (A) and $AsMeI_2$ (B)

bond	ΔE_{Pauli}[a]	ΔV_{elstat}[a]	ΔE_0[a]	ΔE_{orbit}[a]	$BDE_{vertical}$[b]	$BDE_{adiabatic}$[b]	$BDE_{ad(rel)}$[b,c]
A−Bd	634	−401	233	−404	172	21	17
B−B	51	−36	15	−30	15	14	16
A−BB	233	−154	79	−136	57	33	34
AB−B	126	−88	38	−74	36	25[d]	28[d]
A−BBA	365	−237	128	−216	88	45	45
AB−BA[e]	375	−237	138	−234	96	50	62
AB−BA[f]	314	−229	86	−193	107	47	50
A−BB−A	727	−472	255	−435	180	78	78

[a] Terms used are those defined in the analysis scheme of Bickelhaupt and Baerends.[19] In accordance with thermochemical conventions, a negative value indicates an attractive contribution to the interaction in question. [b] BDE(A−B) = E(A) + E(B) − E(AB) (a positive value indicates a positive absolute bond strength). [c] Includes a scalar relativistic correction obtained according to the ZORA formalism.[20,21] [d] Calculated using the optimized "crystal-conformation monomer" geometry. [e] Calculated for dissociation to pyramidal-$AsMeI_2$ adducts. [f] Dissociation to give a pair of planar-$AsMeI_2$ adducts.

weights. It is also noteworthy that the ΔE_{orbit} value for the pair of long, equatorial As−I "bonds" (3.134 Å) is 41 kJ mol^{-1} larger than the corresponding ΔE_{orbit} value for the axial As−I pair, despite the shorter distance (3.024 Å) for the latter interactions. This result indicates that there is more bonding character in the long equatorial As−I interactions than in the short axial interactions, consistent with the observed crystallization of planar (rather than pyramidal) $AsMeI_2$ subunits in these adducts.

According to the Voronoi[28,29] and Mulliken charge distributions for $PhMe_2As{\rightarrow}AsMeI_2$ and $(PhMe_2As{\rightarrow}AsMeI_2)_2$, the As−As interaction is more polar in the monomer than in the dimer; this is true also of all of the As−I interactions. This trend may result from the somewhat shorter contact distances in the monomer than in the dimer, with the result that the electrostatic interaction is stronger in the monomer. This is confirmed by the bond energy contributions listed in Table 5. Note that, due to bond elongation, the "covalent" contributions embodied in ΔE_{orbit} are even more heavily reduced in the monomer than are the electrostatic components (ΔV_{elstat}), consistent with the greater sensitivity to distance generally expected for orbital overlap interactions than for Coulombic effects. Nevertheless, in both monomer and dimer, the $PhMe_2$-As-*As* atom, As(1), in particular shows a larger (positive) charge than in isolated $PhMe_2As$, which is consistent with significant electron donation from this atom to the somewhat delocalized $AsMeI_2$ unit(s).

Finally, examination of the As-centered valence orbitals within the dimer indicates that there is clear bonding character along the As−As axis, but this bonding does not conform to a classical "coordinate covalent" bond since each arsenic atom principally contributes, in approximately equal measure, occupied, rather than virtual, orbital character to the interaction. Nor can the increased coordination number about As(2) be satisfactorily interpreted in terms of hypervalence, because the occupied bonding orbitals involving As(2) show very little d-orbital character (ca. 2%); no significant d character is seen in any of the bonding orbitals involving As(1). Our best interpretation of the heavy-atom bonding within $(PhMe_2As{\rightarrow}AsMeI_2)_2$ is to formulate the structure as $[PhMe_2As{\rightarrow}AsMeI^+I^-]_2$. Note that, although the I(2) atoms in this assignment (the "bridging" iodide ions) show a markedly greater negative charge in the various complexes than in isolated $AsMeI_2$, there is very little charge localization on As(2) or significant As(2) orbital character in the valence orbitals associated with the I(2) atoms. These observations, which suggest that both the ionic and covalent components of the As(2)−I(2) interaction are weak, help to explain why the AB−BA bond dissociation energies (which formally require rupture of two As(2)−I(2) "bonds" to produce either planar- or pyramidal-$AsMeI_2$ complexes as products) are so low, at 25−30 kJ mol^{-1} per bond. Ultimately, the combined fragility of the As(1)−As(2) and As(2)−I(2) bonds is responsible for the tendency of the adduct to dissociate in solution.

Conclusion

The long known, brightly colored adducts $PhMe_2As{\cdot}AsPhI_2$, $PhMe_2As{\cdot}AsMeI_2$, and $PhMeEtAs{\cdot}AsMeI_2$ have structures in the solid state in which the tertiary arsine is coordinated orthogonally to the T-shaped iodoarsine with the As→As distances being 2.46−2.50 Å. The calculated bond energies for the As→As interaction of 10−50 kJ mol^{-1} are consistent with the ready dissociation of the adducts in solution and with the importance of the observed intermolecular As−I···As interactions in stabilizing the crystal lattices of the adducts.

Experimental Section

General Comments. Solvents were purified by conventional methods and stored under nitrogen. Elemental analyses were performed by staff within the Research School of Chemistry.

Syntheses. The adducts $PhMe_2As{\rightarrow}AsPhI_2$, $PhMe_2As{\rightarrow}AsMeI_2$, and $PhMeEtAs{\rightarrow}AsMeI_2$ and their components were prepared and isolated according to the methods described by Burrows and Turner.[1]

$PhMe_2As{\rightarrow}AsPhI_2$: orange prisms from ethanol, mp 36 °C [lit.[1] 69 °C]. Anal. Calcd for $C_{14}H_{16}AsI_2$: C, 28.6; H, 2.7; I, 43.2. Found: C, 28.4; H, 2.6; I, 43.0.

$PhMe_2As{\rightarrow}AsMeI_2$: yellow plates from ethanol, mp 93 °C [lit.[1] 93−94 °C]. Anal. Calcd for $C_9H_{14}AsI_2$: C, 20.6; H, 2.7; I, 48.3. Found: C, 20.7; H, 2.7; I, 48.2.

$PhMeEtAs{\rightarrow}AsMeI_2$: yellow needles from ethanol, mp 84 °C [lit.[1] 84 °C]. Anal. Calcd for $C_{10}H_{16}AsI_2$: C, 22.3; H, 3.0; I, 47.0. Found: C, 22.0; H, 2.9; I, 46.9.

(24) Baerends, E. J.; Autschbach, J.; Bérces, A.; Bo, C.; Boerrigter, P. M.; Cavallo, L.; Chong, D. P.; Deng, L.; Dickson, R. M.; Ellis, D. E.; Fan, L.; Fischer, T. H.; Fonseca Guerra, C.; van Gisbergen, S. J. A.; Groeneveld, J. A.; Gritsenko, O. V.; Gruning, M.; Harris, F. E.; van den Hoek, P.; Jacobsen, H.; van Kessel, G.; Kootstra, F.; van Lenthe, E.; McCormack, D. A.; Osinga, V. P.; Patchkovskiii, S.; Philipsen, P. H. T.; Post, D.; Pye, C. C.; Ravenek, W.; Ros, P.; Schipper, P. R. T.; Schreckenbach, G.; Snijders, J. G.; Sola, M.; Swart, M.; Swerhone, D.; te Velde, G.; Vernooijs, P.; Versluis, L.; Visser, O.; van Wezenbeek, E.; Wiesenekker, G.; Wolff, S. K.; Woo, T. K.; Ziegler, T. *Amsterdam Density Functional*; S.C.M., Vrije Universiteit, Theoretical Chemistry: Amsterdam, The Netherlands, 2004; version 2004.01.

(25) Guerra, C. F.; Snijders, J. G.; te Velde, G.; Baerends, E. *J. Theor. Chem. Acc.* **1998**, *99*, 391−403.

(26) te Velde, G.; Bickelhaupt, F. M.; Baerends, E. J.; Guerra, C. F.; van Gisbergen, S. J. A.; Snijders, J. G.; Ziegler, T. *J. Comput. Chem.* **2001**, *22*, 931−967.

(27) Versluis, L.; Ziegler, T. *J. Chem. Phys.* **1988**, *88*, 322−328.

(28) te Velde, G. Numerical integration and other methodological aspects of band structure calculations in chemistry; Ph.D. thesis, Vrije Universiteit: Amsterdam, 1990.

(29) Bickelhaupt, F. M.; Hommes, N. J. R. V.; Guerra, C. F.; Baerends, E. J. *Organometallics* **1996**, *15*, 2923−31.

Theoretical Methods. Density functional theory calculations were performed on Linux-based Pentium IV computers using the Amsterdam Density Functional (ADF) program, version ADF 2004.01.[24−26] Calculations were performed using the density functionals described in the text: final results use the Perdew−Burke−Ernzerhof gradient-corrected density functional approach.[14] Slater orbital basis sets used in all calculations were of triple-ζ plus polarization quality (TZP). Electrons in orbitals up to and including 1s {C}, 3p {As}, and 4p {I} were treated in accordance with the frozen-core approximation. Optimized geometries were obtained using the gradient algorithm of Versluis and Ziegler.[27] Following geometry optimization, additional calculations were executed to investigate structural and bonding aspects. Single-point all-electron calculations using the ZORA formalism[20,21] were undertaken to evaluate the relativistic corrections to the total energy. Other calculations, neglecting relativistic corrections, implemented a molecular fragment-based approach to characterize individual bond energies between subunits.[15−19] All calculations were performed in a spin-restricted fashion. A methodological assessment, performed using several different DFT methods, is described in the Supporting Information associated with the present work.

Crystal Structures. Single-crystal X-ray diffraction data for the compounds were collected at 200 K using a Nonius Kappa CCD diffractometer. Details are given in Table 1. Data were processed using Denzo and Scalepack software and corrected for absorption. The structures were solved by direct methods (SIR92[12]) and refined by full matrix on F with use of CRYSTALS or RAELS2000.[13] *PhMe*$_2$As→*AsPhI*$_2$: The crystallographic asymmetric unit consists of one $C_{14}H_{16}As_2I_2$ molecule. The crystal studied was partly twinned, partly disordered. The twin-disorder mechanism was identified and involves an alternative choice for the stacking of adjacent layers perpendicular to the *a* axis. Individual layers (x = −1/4 to 1/4 or 1/4 to 3/4) are ordered and have $P2_1$ symmetry. The space group $Pna2_1$ results if adjacent layers are related by an *n* glide perpendicular to *a*. The space group $P2_1/n$ results if adjacent layers are related by an inversion. If each layer has a 1:1 disorder between its two options, the resulting space group is *Pnan*. If the inversion is chosen to be at 1/4, 1/4, 0, the subgroup $Pna2_1$ is in its standard setting. The two possible orientations of any layer in the structure are related by the pseudosymmetry operation $x, -y+1, -z+1/2$ (a symmetry element of *Pnan* but not $Pna2_1$ nor $P2_1/n$). The atom As2 at 0.6504, 0.5149, 0.2469 lies approximately on this 2-fold axis; this operation also relates I1 at 0.6371, 0.2275, 0.2157 to I2 at 0.6473, 0.7988, 0.2837. When it acts on atom As1 at 0.6040, 0.4732, 0.4665 it creates As1′ at 0.6040, 0.5268, 0.0335. This peak was found as the major peak in a difference map of the refinement of an assumed ordered structure and suggested the twin-disorder model and the possibilty of polytypes.

The constrained refinement program RAELS2000 was used for the refinement because it allows the use of a refinable algebra that combines the structure factors of pseudoequivalent reflections to simulate the result of a twin-disorder mechanism acting on a perfectly ordered prototype structure. For this structure

$$I(hkl) = (1-q)\,|(1-p)\,F(hkl) + (-1)^l p\,F(h\text{-}k\text{-}l)|^2 + q|(1-p')\,F(h\text{-}k\text{-}l) + (-1)^l p'\,F(hkl)|^2$$

where the disorder parameter p and the twin parameter q were obtained from the refinement of $F = I^{1/2}$ values after assuming $p' = p$. Final values were $p = 0.032(1)$ and $q = 0.038(1)$. The nonzero value for p allowed the origin along c to be refined to an accuracy of 0.015 Å. This correlates the errors in the z coordinates of individual atoms but has no effect on the errors in bond lengths and angles compared to a perfectly ordered structure. This procedure allowed the refinement of the major component of the disorder, assuming the minor component was the same in every detail except overall orientation of the layer. The resulting high-quality refinement implies that the reliabilty of the geometric parameters is equivalent to those that would have been obtained if a crystal containing no twinning or disorder had been investigated. The refinement of the anisotropic atom displacement parameters was standard except for the phenyl rings. These were refined using 12 parameter, TL models, the centers of action being fixed on the As atoms to which they were attached. H atoms were reincluded in sensible geometric positions after each refinement cycle and given anisotropic atom displacement parameters defined by the atoms to which they were attached. The standard uncertainties given in the tables of bond lengths and angles correctly account for correlation effects. *PhMe*$_2$→*AsMeI*$_2$: The crystallographic asymmetric unit consists of one $C_9H_{14}As_2I_2$ molecule. H atoms were included at idealized positions and were allowed to ride on the atom to which they were attached. Longer contacts between As2 and I atoms of adjacent molecules complete octahedral geometry for As2 and give rise to chains running through the unit cell. *PhMeEtAs*→*AsMeI*$_2$: The crystallographic asymmetric unit consists of one $C_{10}H_{16}As_2I_2$ molecule. The structure was initially refined with all atom sites fully occupied and with no disorder, yielding $R = 0.023$, $R_w = 0.024$, and $S = 1.07$. A difference electron density map at this stage showed one outstanding peak adjacent to I1 that appeared to be an alternative location for this atom; it was subsequently included as I3. The relative occupancies of I1 and I3 were refined, and their anisotropic displacement parameters were constrained to be equal. The final occupancies were 0.948(3) and 0.052(3) and the agreement factors were $R = 0.018$, $R_w = 0.019$, and $S = 1.04$.

Acknowledgment. R.S. and S.B.W. gratefully acknowledge the Australian Research Council (ARC) for financial support.

Supporting Information Available: Crystallographic data and data collection details, atomic coordinates, bond distances and angles, anisotropic thermal parameters, and hydrogen atom coordinates for the three adducts. Theory: Text and tabular details concerning the methodological assessment performed using several different DFT methods. This information is available free of charge via the Internet at http://pubs.acs.org.

OM0580396